ARTICLE NO. 78-1201R

C 80-004

Analysis and Design of Strake-Wing Configurations

00006
20005

John E. Lamar*
NASA Langley Research Center, Hampton, Va.

The technology is still evolving for improving the transonic maneuver capability of strake-wing configurations. Much of the work to date has been of an experimental nature; whereas, the theories that are available to handle vortex-flow aerodynamics have mostly treated wings of constant sweep. Hence, two efforts were undertaken: 1) to extend one method—the suction analogy—to more general configurations and evaluate it by using selected critical planforms; and 2) to develop a procedure for strake planform shaping and test the resulting shape in conjunction with a wing-body. The conclusions from this study are that 1) some improvement has been made in estimating high angle-of-attack longitudinal aerodynamics, and 2) the gothic strake designed with the developed procedure does produce a stable vortex system in the presence of a wing body and flat postmaximum lift characteristics.

Nomenclature

a_l	= constant
$\bar{a}$	= constant, a_l/C_l^2
BD	= breakdown
b	= span of wing, exposed span of strake
b_l	= constant
$\bar{b}$	= constant, b_l/C_l^2
ΔC_D	= drag-due-to-lift coefficient, drag-due-to-lift/$q_\infty S_{\rm ref}$
C_L	= lift coefficient, lift/$q_\infty S_{\rm ref}$
$C^*_{L,\,\rm theory}$	= C_L due to vortex-lift theory that uses a curve-fitted K_v value to arrive at estimates
C_m	= pitching moment coefficient, pithing moment/$q_\infty S_{\rm ref}\bar{c}$: for planar wings about $\bar{c}/4$; for strake-wing-body about 57.19% body length aft of body nose
$\Delta C_p(\theta,\eta)$	= lifting pressure coefficient at θ,η
C_0	= constant
C_l	= constant
c	= local chord
c_r	= root chord
$c_s c$	= local suction force/q_∞
$\bar{c}$	= reference chord
$\tilde{c}$	= characteristic length in augmented vortex lift
K_v	= vortex lift factor
l	= length of leading-edge perimeter
M	= Mach number
N	= number of chordwise lifting pressure modes
$q_0(\eta)$	= coefficient of $\cot(\theta/2)$ lifting pressure function
$q_j(\eta)$	= coefficient of $\sin(j\theta)$ lifting pressure function
q_∞	= freestream dynamic pressure
S	= area
TE	= trailing edge
U	= freestream velocity
x_{le},y_{le}	= distances on the gothic strake right panel that locate its leading edge from the apex: positive x aft, positively toward the right tip
$x_{\rm ref}$	= distance behind apex to moment reference point
x/c	= fractional streamwise distance along a chord
y_b	= spanwise location of leading-edge break
α	= angle of attack
β	= angle of sideslip and $\sqrt{1-M^2}$
θ	= angular distance along local chord; 0 at leading edge; π at trailing edge
Λ	= constant leading-edge sweep angle
$\Lambda_l(\eta)$	= leading-edge sweep angle function
Λ_t	= constant trailing-edge sweep angle
η	= spanwise coordinate in fractions of semispan
η^*	= η value where $c_s c$ vs η changes from linear to constant

Subscripts

BD	= breakdown
inbd	= inboard
le	= leading edge
max	= maximum
outbd	= outboard
ref	= reference
s	= strake
se	= side edge
$\overline{se}$	= augmented side edge
w	= wing

Introduction

MANY hybrid wing planforms have been studied with the idea of using them on supersonic transports or fighters (see, for example, Refs. 1-3). These planforms can be characterized, in general, as either strake-wing or blended strake-wing configurations. It should be noted that the use of the name "strake" is not universally employed for the forward additional area. This area has also been called the glove, fillet, apex region, and leading-edge extension. The strake-wing combinations that have been studied are also known by different names, for example, ogee and double delta.

The aerodynamic advantages of these complex planforms are, in general, twofold: 1) aerodynamic center control with Mach number change and, 2) the utilization of vortex lift. Reference 2 discusses these advantages in relation to the Concorde design. These advantages have been equally as important for maneuvering aircraft, especially the vortex lift feature as evidenced by the recently developed lightweight fighters F-16 and F/A-18, which utilize strake-wing planforms. Furthermore, there is current interest in developing slender hybrid-wing fighter aircraft which would combine good supersonic cruise performance with higher levels of transonic-maneuver lift. Because of the difficulty in maintaining attached flow for this class of aircraft, vortex lift may also be used here to advantage.

Presented as Paper 78-1201 at the AIAA 11th Fluid and Plasma Dynamics Conference, Seattle, Wash., July 10-12, 1978; submitted Oct. 6, 1978; revision received May 11, 1979. This paper is declared a work of the U.S. Government and therefore is in the public domain. Reprints of this article may be ordered from AIAA Special Publications, 1290 Avenue of the Americas, New York, N.Y. 10019. Member price $2.00 each, nonmember, $3.00 each. **Remittance must accompany order.**

Index categories: Computational Methods; Configuration Design.

*Aeronautical Research Scientist. Associate Fellow AIAA.

Table 1 Double-delta family geometric features

Model number	S,m^2	b, cm	c_r,cm	$\bar{c}$,cm	y_b,cm	x_{ref},cm	Λ_{inbd},deg	Λ_{outbd},deg	Λ_t, deg
1	0.1612	50.80	82.87	47.67	8.05	47.12	80	65	0
2	0.1526	38.10	82.87	49.85	8.05	45.48	80	65	0
3	0.1316	38.10	71.87	42.67	8.05	43.89	80	65	30
4	0.0967	16.10	82.87	62.93	...	35.67	80	65	0
5	0.1240	50.80	68.20	38.27	8.05	43.78	80	65	30

It is to the high subsonic-transonic design problems posed by the supercruising-fighter aircraft that this paper is addressed. For many of the simpler wing geometries, nonhybrid configurations, the vortex lift can be estimated well with available theory (see Refs. 4 and 5, for example). However, success with the slender hybrid-wing, strake-wing configurations, is more limited.

This paper is divided into two sections. The first addresses systematic experimental studies and analysis to assess a current estimating capability for planar strake-wing lift and pitching moment. The second is concerned with developing a procedure for strake design, integrating the result with a wing, and testing the configuration on a fuselage, having dual balances, to high angles of attack. This strake design work only addresses high lift/vortex stability, and not the impact of strake shape in post-breakdown aircraft longitudinal stability or lateral stability at any attitude.

Strake-Wing Analysis

The few strake-wing examples that have appeared in the literature have had their lift[6,7] and pitching moment[8] reasonably well estimated. An exception was a supercruise configuration of Ref. 9. However, that particular configuration did not provide a good basis upon which to judge the adequacy of the estimating tools because 1) the outer panel vortex flow broke down around ≈ 24 deg angle of attack, and 2) the trailing-edge notch effect reduced the attainable lift levels. Therefore, it was decided to perform a systematic wind-tunnel and analytical study using the configurations of Fig. 1 to determine if there was an approach based on the geometry variables that could lead to the measured results. The technique pursued is that of potential flow calculations coupled with the suction analogy and includes as variables: 1) the spanwise extent of leading-edge suction, 2) trailing-edge notch ratio, and 3) the augmented vortex lift[4] where appropriate.

The wind-tunnel study employed the five models (numbered 1-5) shown in Fig. 1. Note that three of them were obtained by interchanging trailing-edge pieces (models 1-3). The basic strake-wing configuration (model 1) has an 80 deg inboard sweep, 65 deg outboard sweep, pointed tip, and an unswept trailing edge. This planform should not experience the outboard wing leading-edge vortex bursting problem described for the configuration of Ref. 9 because of the higher outboard sweep. Reference 10 indicates that vortex breakdown does not occur ahead of the trailing edge until the angle of attack is about 32 deg. The other four models in this series each provide a slightly different experimental and analytical situation. For example, model 5 has the same leading-edge shape and pointed tip, but a swept trailing edge. Two others have similar leading edges, but model 2 has an unswept trailing edge with a cropped tip, while model 3 has both a swept trailing edge and cropped tip. Model 4 has only the inboard sweep with a cropped tip extending from the original streamwise position of the cranked leading edge to the planform trailing edge. This configuration represents a strake wing in which the entire wing is removed outboard of the leading-edge break. Pertinent geometrical quantities for these models are given in Table 1.

The models were essentially planar with symmetrically beveled edges and had the balance housing located symmetrically as well. A triangular fin was welded along the entire lower-surface centerline for lateral stability. The models were tested on a standard sting arrangement at two different knuckle angles to provide an angle-of-attack range from $\approx$-3 to ≈ 32 deg with about 10 deg overlap starting near 10 deg. Only a low-subsonic Mach number (≤ 0.20) was used in the test.

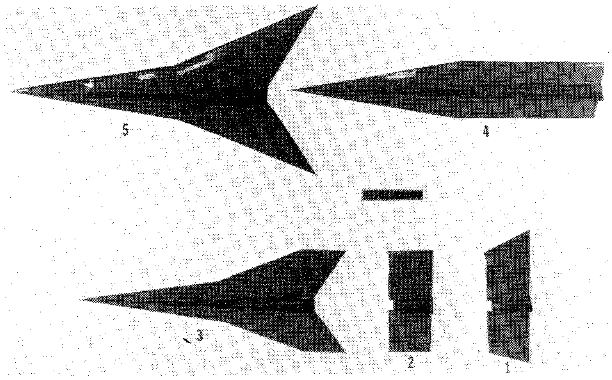

Fig. 1 Five planforms in double-delta family.

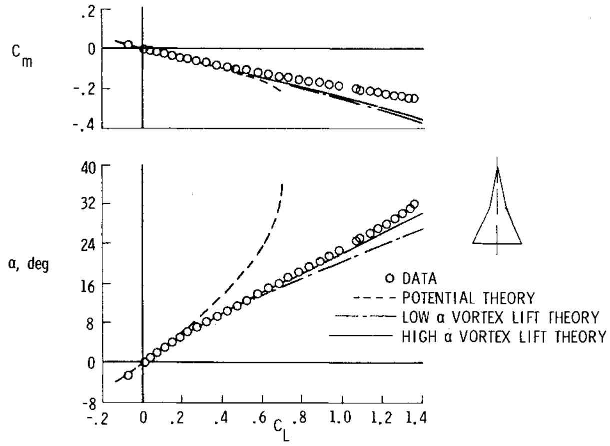

Fig. 2 Double-delta theoretical and experimental longitudinal aerodynamic characteristics, model 1, $M \approx 0$.

Data and analytical results for α vs C_L and C_m vs C_L are presented in Figs. 2-6. ΔC_D vs C_L results are not presented, because for these wings, if the α vs C_L are well estimated, so will be the ΔC_D vs C_L. Before the results are discussed, the different analytical methods will be described.

At most, there are four analytical curves for each set of data. The curves are: 1) potential theory at zero suction; 2) original vortex-lift theory; 3) low-α vortex-lift theory; and 4) high-α vortex-lift theory. They were all obtained using the Vortex Lattice Method of Ref. 11. When only three curves appear, it may be because the original and high-α vortex-lift theories are coincident as for model 1 or the high- and low-α vortex-lift theories are coincident as for model 4. The potential theory and the original vortex-lift theory have been described in several references, including Ref. 6. Briefly though, the potential theory, at zero suction, is just the potential flow normal force computational solution with

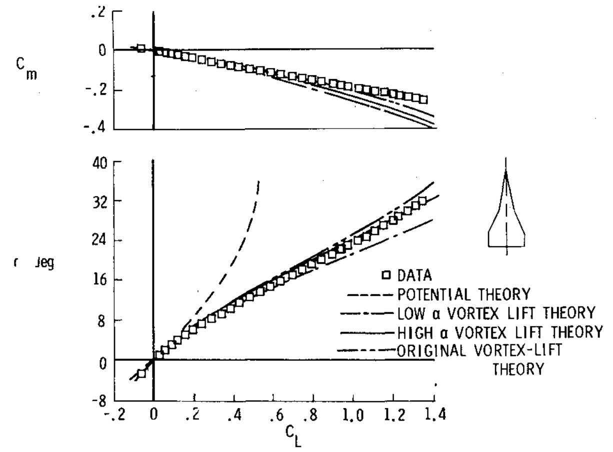

Fig. 3 Double-delta theoretical and experimental longitudinal aerodynamic characteristics, model 2, $M \approx 0$.

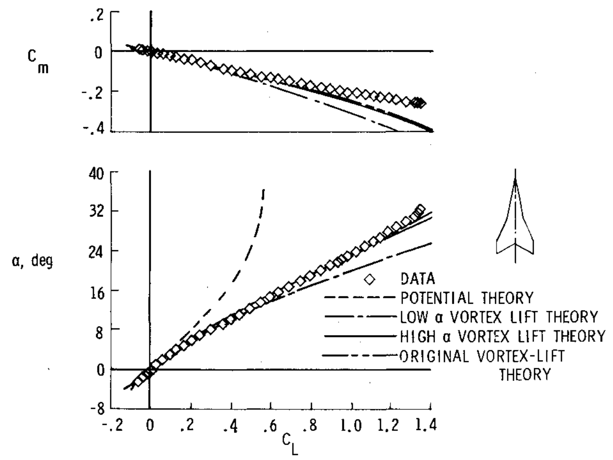

Fig. 4 Double-delta theoretical and experimental longitudinal aerodynamic characteristics, model 3, $M \approx 0$.

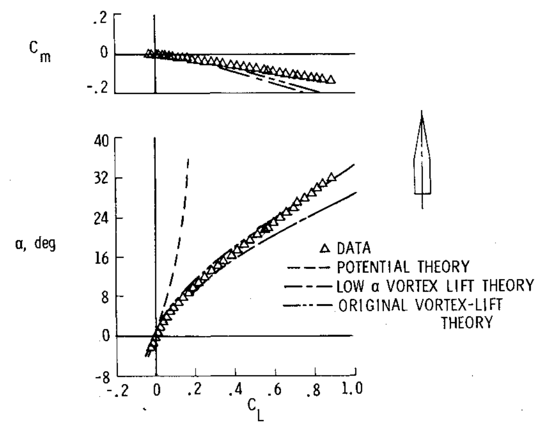

Fig. 5 Double-delta theoretical and experimental longitudinal aerodynamic characteristics, model 4, $M \approx 0$.

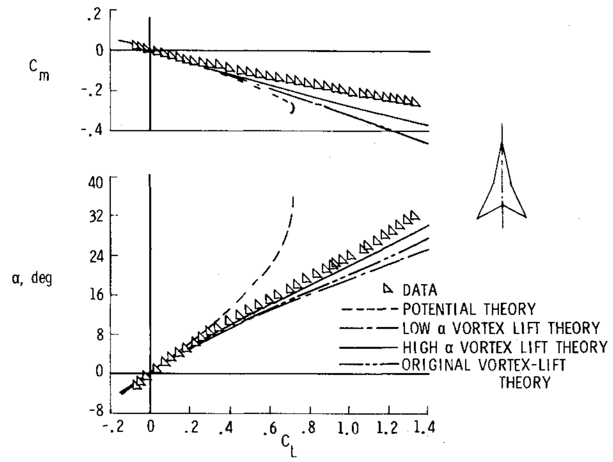

Fig. 6 Double-delta theoretical and experimental longitudinal aerodynamic characteristics, model 5, $M \approx 0$.

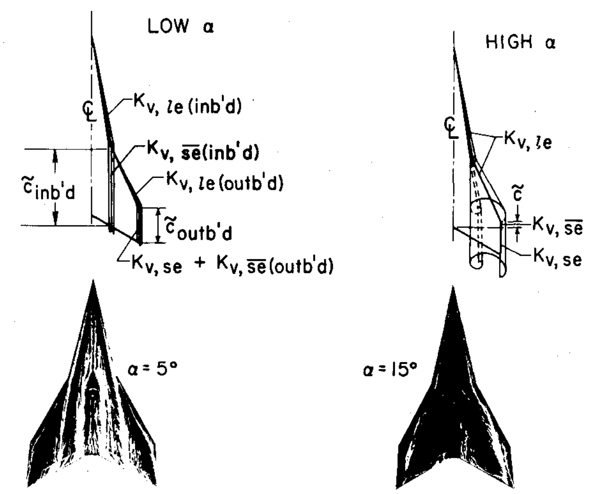

Fig. 7 Vortex flow modeling methods for double deltas, suction analogy, and augmented vortex-lift applications.

appropriate trigonometric terms. The terminology for the original vortex-lift theory includes, herein, both the leading-edge and side-edge suction terms and their contributions, through the suction analogy, to vortex-flow aerodynamics. The other two theories are the better of those devised and are described with the aid of Fig. 7.

For a representative cropped double-delta-type wing, Fig. 7 shows how the vortex-flow aerodynamics are modeled at both low and high angles of attack. The necessity for this α-dependent flow modeling comes from a study of surface oil flow patterns, which are also shown for two representative α's. The oil flows consistently show here, and for all double-deltas tested, evidence of two primary vortex systems at low α's, whereas, only one is of consequence at high α's.

At low α's, the leading-edge vortex from the inboard wing panel passes over the root chord of the outboard wing panel. Augmented vortex-lift estimates are made based on $K_{v,le(\text{inbd})}$ and $\tilde{c}_{\text{inbd}}$, or $K_{v,\overline{se}(\text{inbd})}$. Additional augmented vortex lift is available at the tip due to the action of the outboard leading-edge vortex, i.e., $K_{v,le(\text{outbd})}$ and $\tilde{c}_{\text{outbd}}$, or $K_{v,\overline{se}(\text{outbd})}$. Therefore, the low-α vortex-lift theory combines the original vortex-lift theory with the other two contributors to vortex-flow aerodynamics.

At high α's, the assumption is that the one primary vortex system acts over the outer panel in a manner similar to that described in Ref. 4 for the original augmented vortex-lift application (see also Ref. 12). Thus, with the increasing size of the vortex and the more inboard location of the reattachment line, coupled with the loss in lift due to the loss of flow reattachment area through trailing-edge notching, the original $\tilde{c}$ definition is used as shown. This $\tilde{c}$ in conjunction with the entire leading-edge contribution to $K_{v,le}$ provides $K_{v,\overline{se}}$. Therefore, combining the original vortex-lift theory with contributions to vortex flow aerodynamics from $K_{v,\overline{se}}$ produces the high-α vortex-lift theory.

Returning to Figs. 2-6, it is clear that, in general, the low-α vortex-lift theory does offer improvements in C_L estimation up to 8 deg over the original theory. At higher α's, improvements are noted only for models 2 and 5. For the pitching moment, not much effect is noted at low C_L; however, at high C_L, improvements in C_m estimation are noted for models 1 and 5. Additional improvements may possibly be obtained at the higher α's, if only a fraction of the leading- and side-edge vortex-lift flow aerodynamics from the outboard panel are included. This could be justified on the premise that the inner and outer panel vortex systems may not merge, as assumed; instead, the outer panel vortices may be displaced vertically, thereby reducing their influence. This was not anticipated nor confirmed by oil flows for these wings because, unlike the strake-wing-body configurations which follow, the difference in the two sweep angles was not too large, only 15 deg. The potential theory curves are only given for reference.

The conclusion from this section is that, although some improvements have been made in the α vs C_L and C_m vs C_L estimating capability, these improvements are α and configuration dependent.

Having made some progress in the realm of the improved estimation of α vs C_L and C_m vs C_L for strake wings; the problem of strake design will be addressed.

Strake Design

The problem in strake design is to find a starting place. Does one pick conventional shapes that are known to have reasonably good vortex-flow characteristics and reach large angles of attack and lift coefficients before breakdown occurs ahead of the trailing edge, as with the highly swept delta and low aspect ratio, rectangular wing, or does one try to find "better shapes," and, if so, by what means other than experimental?

It should be pointed out that the significance of vortex breakdown occurring ahead of the trailing edge is directly related to the α at which $C_{L_{max}}$ is developed, as shown in Fig. 8 for a 70 deg delta wing. This is further documented by Wentz in Ref. 10 for other slender delta wings having $\Lambda > 70$ deg.

The information presented in this section details a design approach based on trying to establish a "better shape," by using as a basis the correlating idea that "better shapes" are those which have higher values of the potential-flow suction distribution near the tip. This may be interpreted in a physical sense for the separated flow in that the flowfields are more stable for shapes that have higher levels of separation-induced vorticity near the tip. Reference 4 first noted the potential-flow correlation for simple delta wings, and Fig. 8 shows the effect of increasing sweep on both the peak and $\alpha_{BD\text{-}TE}$.

To develop a strake planform from the suction distribution is just the reverse of what has been presented so far; that is, an existing vortex lattice method (VLM) analysis code[11] being applied to a given geometry. This reversed problem first must

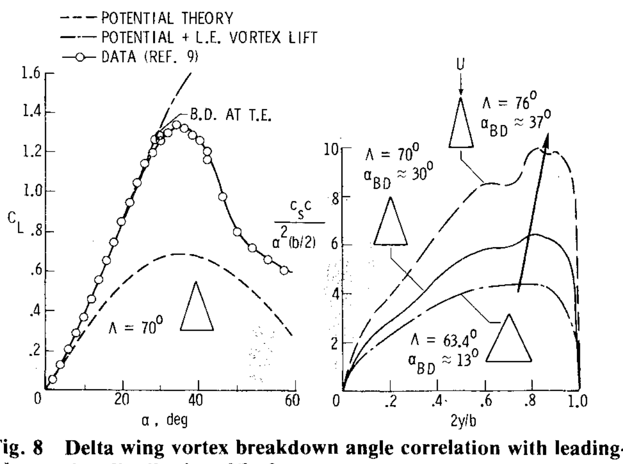

Fig. 8 Delta wing vortex breakdown angle correlation with leading-edge suction distribution, $M \approx 0$.

be formulated, then the assumptions that are needed to effect a solution must be made, and lastly, a level of confidence in the answers must be established by example. To work this problem, attached-flow concepts will be used.

For an attached-flow pressure distribution given by

$$\Delta C_p(\theta,\eta) = \frac{2q_0(\eta)}{q_\infty c}\cot\frac{\theta}{2} \sum_{j=1}^{N-1} \frac{2q_j(\eta)}{q_\infty c}\sin j\theta$$

the local suction distribution can be found from Ref. 13 to be

$$c_s c = \frac{\sqrt{\beta + \tan^2\Lambda_l(\eta)}}{2\pi\cos\Lambda_l(\eta)} \left(\frac{2q_0(\eta)}{q_\infty c}\right)^2 c$$

This equation relates the local leading-edge sweep angle $\Lambda_l(\eta)$ and chord c through the suction distribution $c_s c$ and coefficient of the $\cot(\theta/2)$ term in $\Delta C_p(\theta,\eta)$. We have another relationship between $\Lambda_l(\eta)$ and c, and it is

$$c(\eta) = c_r - (b/2)\int_0^\eta \tan\Lambda_l(\bar{\eta}) - \tan\Lambda_t)\,d\bar{\eta}$$

However, to obtain a solution, some assumptions will be needed with regard to $c_s c$ and $\Delta C_p(\theta,\eta)$. For example, the correlation between suction distributions which peak toward the tip and the resulting large values of $\alpha_{BD\text{-}TE}$ could be used. This can be done by assuming that

$$c_s c = (a_l + b_l\eta)\,b/2$$

The second assumption would be that since the planar strakes are designed to produce separated flow with reattachment (i.e., vortex flow), the associated leading-edge pressures must conceptually, as well as in reality, exceed an unspecified limiting value beginning at some small angle of attack. This means that for the attached-flow pressure distribution, the region of interest is near the leading edge, i.e., θ and x/c being small values. Hence, for this problem we could take

$$\Delta C_p(\theta,\eta) \approx \frac{2q_0(\eta)}{q_\infty c}\cot\frac{\theta}{2}$$

If an additional assumption is made that across the span

$$\Delta C_p(\theta,\eta) = \text{const} = C_0$$

at constant θ or x/c, we no longer have a real three-dimensional attached or potential flow but a somewhat related flow† in which the problem will be solved. This also meant that the sectional lift contribution from the $\cot\theta/2$ term is constant. Thus,

$$\frac{2q_0(\eta)}{q_\infty c} \approx \text{const} = C_l$$

The preceding discussion implies that if the flow separates anywhere, it separates everywhere simultaneously. Putting all of the assumptions together yields

$$(a_l + b_l\eta)\left(\frac{b}{2}\right) = \frac{\sqrt{\beta^2 + \tan^2\Lambda_l(\eta)c}}{2\pi\cos\Lambda_l(\eta)}(C_l)^2$$

†Other assumptions concerning $\Delta C_p(\theta,\eta)$ and θ could be made. For example, 1) $\Delta C_p(\theta,\eta)$ could be kept constant at a fixed distance behind the leading edge or 2) $\Delta C_p(\theta,\eta)$ could take on a three-dimensional variation at constant θ. Either one of these would impact the resulting description of the leading edge.

or

$$(\bar{a}+\bar{b}\eta)\left(\frac{b}{2}\right)=\frac{\sqrt{\beta^2+\tan^2\Lambda_l(\eta)}}{2\pi\cos\Lambda_l(\eta)}\left[c_r-\frac{b}{2}\int_0^\eta(\tan\Lambda_l(\bar{\eta})-\tan\Lambda_t)\mathrm{d}\bar{\eta}\right]$$

where

$$\bar{a}=a_l/C_l^2 \text{ and } \bar{b}=b_l/C_l^2$$

At $\eta=0$, the initial sweep of the strake can be determined by

$$\Lambda_l(\eta=0)=\sin^{-1}\left[\left(\frac{c_r^2M^2}{2\pi^2\bar{a}^2b^2}+1-\frac{\sqrt{M^4c_r^4+4\pi^2\bar{a}^2b^2c_r^2}}{2\pi^2\bar{a}^2b^2}\right)^{1/2}\right]$$

For $\eta>0$, $\Lambda_l(\eta)$ must be solved by iteration from the following initial value problem

$$c_r-\frac{(\bar{a}+\bar{b}\eta)(b/2)2\pi}{\sqrt{\beta^2\sec^2\Lambda_l(\eta)+\sin^2\Lambda_l(\eta)\sec^4\Lambda_l(\eta)}}=\frac{b}{2}\int_0^\eta(\tan\Lambda_l(\bar{\eta})-\tan\Lambda_t)\mathrm{d}\bar{\eta}$$

This solution has been coded for the CDC 6000 series digital computer and typically executes in 1-2 s for a single set of parameters.

It can be seen that the solution for $\Lambda_l(\eta)$ and later c are dependent on $\bar{a}$, $\bar{b}$, b, Λ_t, c_r, and β^2 or $(1-M^2)$. The effect of M has been calculated to be slight for a characteristic $\bar{a}$ and $\bar{b}$; hence, only $M=0$ will be used herein.

The 76 delta suction distribution of Fig. 8 will be used as a model since it produced a large $\alpha_{BD\text{-}TE}$ value. Values of a_l and b_l associated with this distribution are 1 and 12, respectively, for $C_l^2=1$. However, early usage with these numbers led to very small values of $\Lambda_l(\eta)$, especially near $\eta=0$, making it seem unlikely that a strong vortex system would be produced. Therefore, smaller values of C_l^2 were tried until the resulting $\Lambda_l(\eta)$ distribution appeared reasonable. $C_l^2=0.25$ was determined to be small enough for this a_l and b_l. It should be mentioned here that since the starting suction distribution was the result of a three-dimensional solution for the 76 deg delta wing and the $\Delta C_p(\theta,\eta)$ distribution assumed herein is not three-dimensional, one should not expect the 76 deg delta wing to emerge as the solution. Another representation of the suction distribution which has large values near the tip is obtained by truncating the same linear form part-way out the span, at $\eta^*\cdot b/2$, and by letting the suction be constant from there to the tip. This was tried and the $\Lambda_l(\eta)$ results were compared with those of not truncating and the differences were determined to be slight for $\eta^*=0.65$.

Therefore, a first test of this procedure to design a strake planform used the following variables: $a_l=1$, $b_l=12$, $C_l^2=0.25$,‡ $M=0$, $\eta^*=0.65$, and $\Lambda_t=44$ deg.

Λ_t was set to 44 deg because the strake was to abut a 44 deg trapezoidal wing. The resulting shape is gothic (see Table 2 for coordinates), as can be seen at the left of Fig. 9, along with its resulting three-dimensional suction distribution, labeled 3-D ALONE. A comparison of this distribution with the prescribed one shows that even with the assumed pressure distribution being constant across the span near the leading edge—a gross assumption—the resulting strake shape produces a suction peak outboard. Before comparing with the other curve, a description of the strake-wing-body configuration will be given. (A description of the wing-body is given in Ref. 14.)

‡This is equivalent to $a_l=4$, $b_l=48$, and $C_l^2=1$, which is used in Fig. 9.

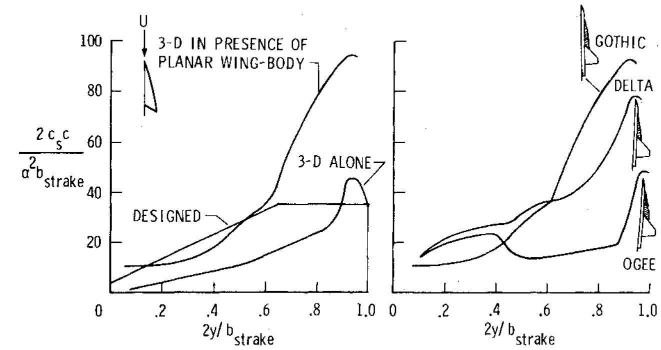

Fig. 9 Strake and strake-wing leading-edge suction distributions, $\Lambda=44$ deg, $M\approx0$.

In order to obtain a near-optimum gothic strake semispan for this configuration, the following study was done. Similar gothic strakes, ranging in semispan from 0.1 to 0.5 of the wing semispan, had their suction distributions calculated in the presence of the wing using the VLM code. The one which was best overall had a semispan ratio of 0.3. To maintain the strake-to-wing semispan relation on the strake-wing-body combination, it was decided to use the exposed wing semispan to set the strake semispan. This effectively made the strake-to-wing semispan ratio larger than 0.3, but avoided having a part of the strake geometry covered up by the body in computations, (planar body representation) and experimental study.

The resulting suction distribution is graphed on the left of Fig. 9 and shows the large upwash influence that the wing has on the gothic strake. The influence is most apparent over the outermost 50% of strake semispan. This same curve is reproduced on the right of Fig. 9 for comparison with suction distributions resulting from a delta strake of the same chord and span, and the large ogee strake described in Ref. 15. It is interesting to note from this figure that the suction distribution peaks are in an order which indicates the gothic strake to be a better shape. Delta strakes of this slenderness are known to have good vortex-breakdown characteristics, and from Ref. 15 it was determined that this ogee strake worked well to $\alpha\approx22$ deg. All three strake-wing-body configurations have been wind-tunnel tested. However, before these results are discussed, sample water-tunnel photographs§ of a slightly smaller-scaled version of the designed gothic strake attached to a 50 deg cropped delta wing are presented for two different angles of attack at zero sideslip (Figs. 10 and 11). Additional water-tunnel photographs, which are of a delta strake having the same span and slenderness ratio as the gothic strake and mounted on the same wing, are shown for comparison.

In the photographs, dark colored water was introduced near the strake apex by means of a dye probe to highlight the path of the vortex core. The comparative photographs at $\alpha=15$ and 25 deg show that the gothic strake promoted a vortex core which could persist farther into the wing pressure field before breaking down than could the delta strake of the same slenderness. These early water-tunnel results of the designed gothic strake were encouraging and preceded the wind-tunnel tests reported herein.

Figures 12 and 13 present the overall strake-wing-body C_L and C_m for the designed gothic strake, a delta strake of the same ratio of exposed semispan to $(c_r)_s$, 0.166, and a group

§The photographs were taken by the Northrop Corporation in their water tunnel and provided to NASA Langley Research Center because of a mutual interest in improving the stability of the strake vortex on strake-wing configurations.

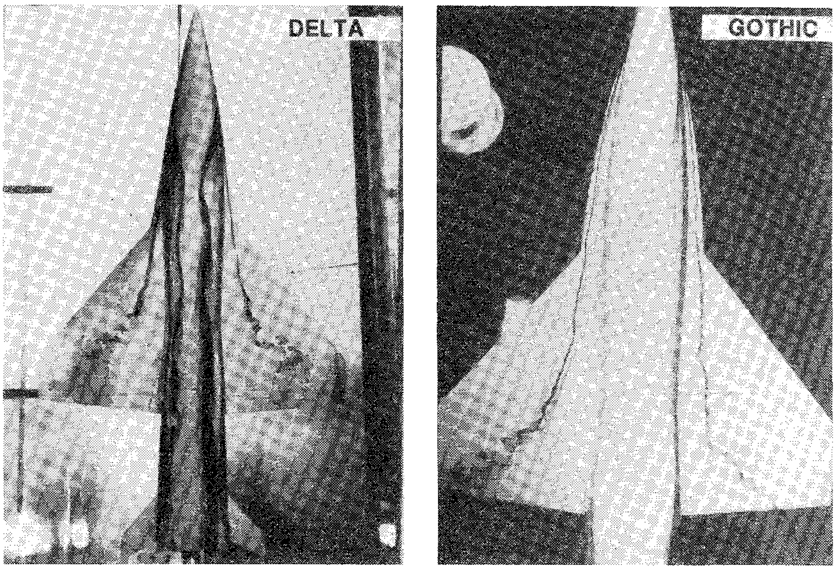

Fig. 10 Effect of strake shape on vortex breakdown, Northrop water-tunnel results $\alpha = 15$ deg, $\beta = 0$ deg.

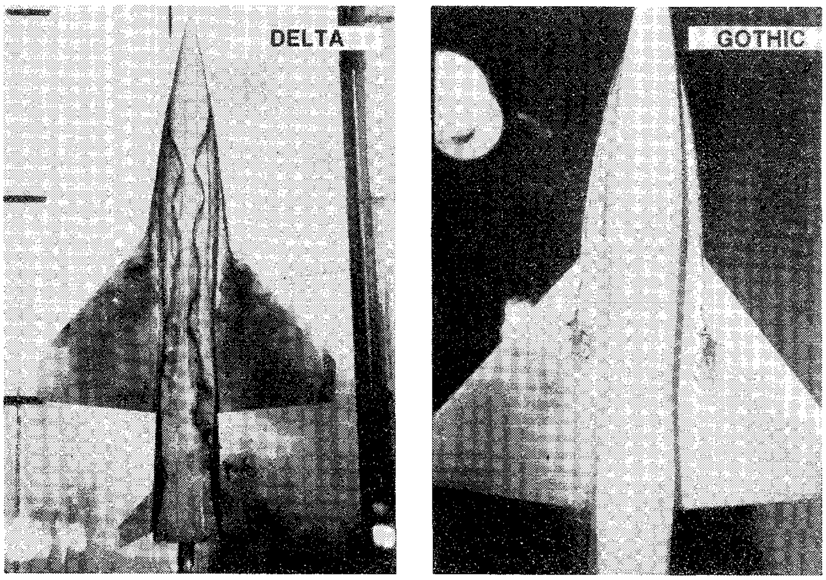

Fig. 11 Effect of strake shape on vortex breakdown, Northrop water-tunnel results, $\alpha = 25$ deg, $\beta = 0$ deg.

of ogee strakes all tested at subsonic speeds on a two-balance agreement of a high-α sting system. The ogee strakes range in ratio of exposed semispan to $(c_r)_s$ from 0 to 0.237 with the larger one being compared with the other two shapes because it performed best, in terms of interference lift, of all ogees tested.[15] Examining the C_L variations first, it can be seen from the left side of Fig. 12 that over the initial α range, the effect of the strake shape is not very important, but becomes so near $C_{L,\max}$. For instance, the ogee strake configuration reaches its $C_{L,\max}$ at the lowest α and after a dropoff retains a constant level; whereas, once the delta strake configuration reaches its $C_{L,\max}$, a higher value, the C_L continues to fall and reaches the level of the ogee strake configuration. The gothic strake configuration reaches comparable values $C_{L,\max}$ with that of the delta strake configuration, after which the high value of C_L reached is better maintained.

For nearly the same ratio of exposed semispan to $(c_r)_s$, the middle-sized ogee strake configuration on the right has similar

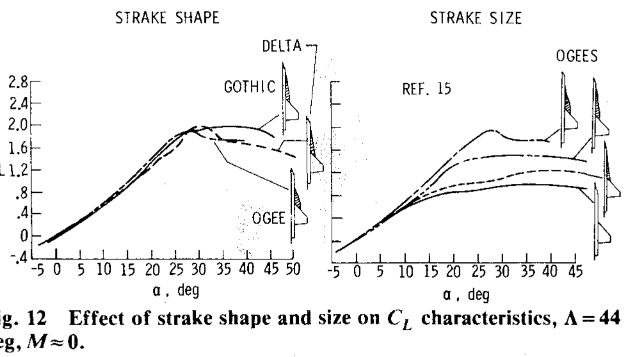

Fig. 12 Effect of strake shape and size on C_L characteristics, $\Lambda = 44$ deg, $M \approx 0$.

Table 2 Gothic strake leading-edge description[a]

x_{le},cm	y_{le},cm	x_{le},cm	y_{le},cm
0	0	15.212	3.562
0.659	0.324	17.432	3.886
1.501	0.648	19.831	4.210
2.496	0.972	22.398	4.534
3.631	1.295	25.111	4.858
4.897	1.619	28.010	5.182
6.291	1.943	31.162	5.505
7.811	2.267	34.691	5.829
9.458	2.591	38.891	6.153
11.235	2.915	45.365	6.477
13.151	3.239		

[a] Exposed wing semispan is 21.59 cm; overall wing span is 50.80 cm.

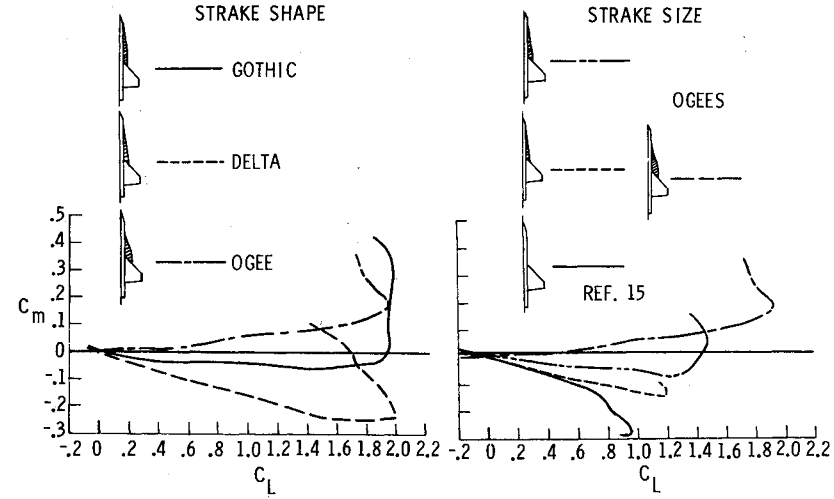

Fig. 13 Effect of strake shape and size on C_m characteristics, $\Lambda = 44$ deg, $M \approx 0$.

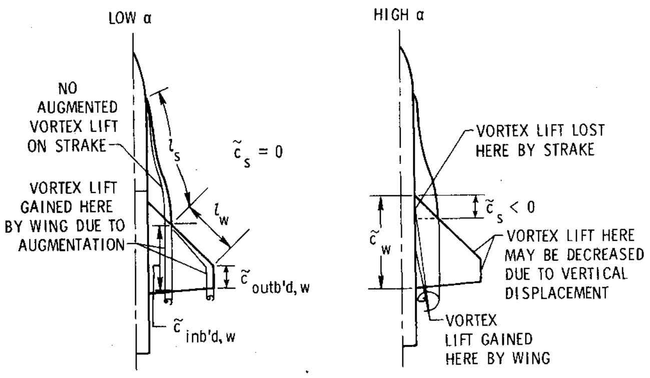

Fig. 14 Theoretical vortex-lift parameters for strake wing.

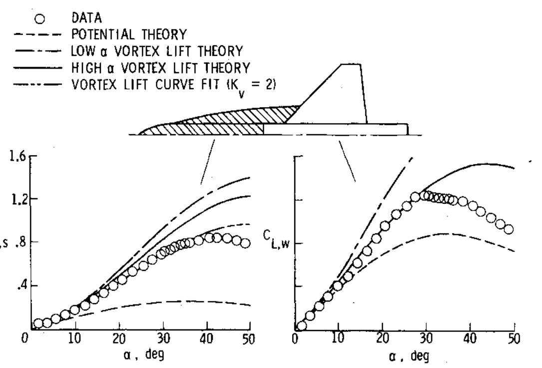

Fig. 15 Estimates of strake and wing lift, $M \approx 0$.

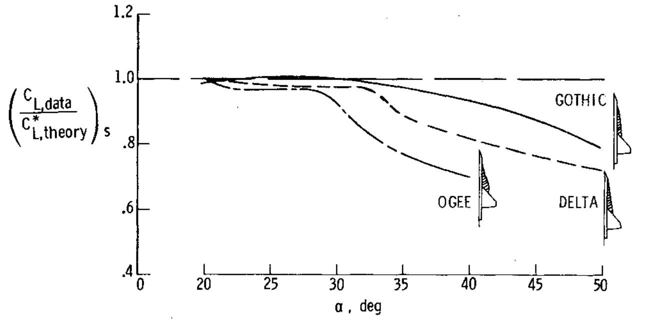

Fig. 16 Effect of strake shape on $C_{L,s}$ characteristics at high α, $\Lambda = 44$ deg, $M \approx 0$.

post-$C_{L,\max}$ characteristics as that of the gothic strake configuration, but at an overall reduced C_L level. This difference is associated with that of strake area and shape. However, for the ogee strake configurations on the right, it is clear that the larger the strake, the higher the $C_{L,\max}$, and increasing the ratio of exposed semispan to $(c_r)_s$ beyond that of the middle strake does not improve the post $C_{L,\max}$ characteristics.

The C_m vs C_L curves on Fig. 13 are organized the same way as the C_L vs α curves on the figure just discussed. All strake-wing curves show pitchup occurring, but it is most severe on the gothic strake configuration because of the slow progression of vortex breakdown on the strake, as shown by the water-tunnel photographs. This slow progression led to the relatively flat post-$C_{L,\max}$ behavior of its C_L vs α curve.

To get an idea of how well the C_L characteristics could be estimated for the gothic strake configuration, the strake or forebody C_L and wing C_L have been separated using tests data and are compared with various vortex-lift theories. The augmented lift concept described originally in Ref. 4 and advanced in collaboration with Luckring[15] for the ogee strake configuration is also employed here, a descriptive figure of which is presented for completeness (Fig. 14). Figure 15 shows both the low- and high-α vortex-lift theories to overpredict the strake C_L, whereas, the high-α vortex-lift theory estimates reasonably well the wing C_L until vortex breakdown occurs. In order to determine the degree to which vortex breakdown effects reduce the lift on the strake, it was necessary to accurately extrapolate the prebreakdown lift effectiveness to higher α's. This was done by extracting for the gothic strake, using a curve-fitting technique, a K_v value. It was determined to be 2.0. This procedure was also employed for the delta strake configuration.

The ratio of the strake C_L data to the curve-fitted vortex-flow theory, $C^*_{L,\text{ theory}}$, is presented in Fig. 16 for the previously mentioned strakes along with the largest ogee strake configuration, whose data were well estimated by the high-α vortex-flow theory. This figure shows the gothic strake to retain more of its vortex lift at higher α's than either of the other strakes and, moreover, to lose that lift less suddenly than the others. That explains why the total C_L for the gothic strake configuration is fairly constant for $\alpha > 38$ deg in Fig. 12, even though the wing lift falls off rapidly in that α range.

Concluding Remarks

In the general area of strake-wing analysis and design, some progress has been made in extending the suction analogy to estimate overall lift and pitching moment for configurations other than double delta, in particular, double arrow. With regard to strake design, the procedure described herein produced a gothic strake which, in conjunction with a wing-body, developed a well-behaved vortex system resulting in a flat postmaximum lift variation with increasing angle of attack. In addition, available water-tunnel photographs indicate that the gothic strake produces a vortex system that is better able to penetrate the wing pressure field than a delta strake of the same span and slenderness.

References

[1] Lamar, J.E. and Alford, W.J. Jr., "Aerodynamic-Center Considerations of Wings and Wing-Body Combinations," TN D-3581, NASA, Oct. 1966.

[2] Morgan, Sir Morien, "A New Shape in the Sky," *Aeronautical Journal*, Jan. 1972, pp. 1-18.

[3] Ray, E.J., "NASA Supersonic Commercial Air Transport (SCAT) Configuration: A Summary and Index to Experimental Characteristics," TM X-1329, NASA, Jan. 1967.

[4] Lamar, J.E., "Some Recent Applications of the Suction Analogy to Vortex-Lift Estimates," in *Aerodynamic Analysis Requiring Advanced Computers*, SP-347, NASA, March 1975.

[5] Lamar, J.E. and Luckring, J.M., "Recent Theoretical Developments and Experimental Studies Pertinent to Vortex Flow Aerodynamics—With a View Towards Design," in *High Angle of Attack Aerodynamics*, CP 247, AGARD, Jan. 1979.

[6] Polhamus, E.C., "Prediction of Vortex-Lift Characteristics by a Leading-Edge Suction Analogy," *Journal of Aircraft*, Vol. 8, April 1971, pp. 193-199.

[7] Bradley, R.G., Smith, C.W., and Bhateley, I.C., "Vortex-Lift Prediction for Complex Wing Planforms," *Journal of Aircraft*, Vol. 10, June 1973, pp. 379-381.

[8] Smith, C.W., Bradley, R.G., and Bhateley, I.C., "Vortex Lift, Drag, and Pitching Moment Predictions for Sharp-Edged Wings With Camber," General Dynamics—Convair Aerospace Division ERR-FW-1470, Dec. 1973.

[9] Campbell, J.F., Gloss, B.B., and Lamar, J.E., "Vortex Maneuver Lift for Super-Cruise Configurations," TM X-72836, NASA, Feb. 1976.

[10] Wentz, W.H. Jr. and Kohlman, D.L., "Wind Tunnel Investigations of Vortex Breakdown on Slender Sharp-Edged Wings," CR-98737, NASA, 1968.

[11] Lamar, J.E. and Gloss, B.B., "Subsonic Aerodynamic Characteristics of Interacting Lifting Surfaces with Separated Flow Around Sharp Edges Predicted by a Vortex-Lattice Method," TN D-7921, NASA, Sept. 1975.

[12] Lamar, J.E., "Recent Studies of Subsonic Vortex Lift Including Parameters Affecting Stable Leading-Edge Vortex Flow," *Journal of Aircraft*, Vol. 14, Dec. 1977, pp. 1205-1211.

[13] Wagner, S., "On the Singularity Method of Subsonic Lifting-Surface Theory," AIAA Paper 69-37, New York, 1969.

[14] Gloss, B.B., "The Effect of Canard Leading-Edge Sweep and Dihedral Angle on the Longitudinal and Lateral Aerodynamic Characteristics of a Close-Coupled Canard-Wing Configuration," TN D-7814, NASA, Dec. 1974.

[15] Luckring, J.M., "Theoretical and Experimental Aerodynamics of Strake-Wing Interactions Up to High Angles-of-Attack," AIAA Paper 78-1202, Seattle, Wash., July 1978.